Octahedral connectivity and its role in determining the phase stabilities and electronic structures of low-dimensional, perovskite-related iodoplumbates

Zeyu Deng, Gregor Kieslich, Paul D. Bristowe, Anthony K. Cheetham, and Shijing Sun

Citation: APL Materials **6**, 114202 (2018); doi: 10.1063/1.5046404
View online: https://doi.org/10.1063/1.5046404
View Table of Contents: http://aip.scitation.org/toc/apm/6/11
Published by the American Institute of Physics

Octahedral connectivity and its role in determining the phase stabilities and electronic structures of low-dimensional, perovskite-related iodoplumbates

Zeyu Deng,[1] Gregor Kieslich,[2] Paul D. Bristowe,[1,a] Anthony K. Cheetham,[1,a] and Shijing Sun[1,3,a]

[1]*Department of Materials Science and Metallurgy, University of Cambridge, Cambridge CB3 0FS, United Kingdom*
[2]*Department of Chemistry, Technical University of Munich, D-85748 Garching, Germany*
[3]*MIT Photovoltaic Research Laboratory, Massachusetts Institute of Technology, 77 Massachusetts Avenue, Cambridge, Massachusetts 02139, USA*

(Received 27 June 2018; accepted 22 August 2018; published online 11 September 2018)

We describe a single crystal X-ray diffraction study and computational analysis of three guanidinium (Gua) based low-dimensional iodoplumbates with one edge-sharing and two corner-sharing octahedral connectivities, respectively. $(Gua)_3PbI_5$, which is reported for the first time, has a 1D corner-sharing octahedral chain structure. $GuaPbI_3$ adopts a 1D edge-sharing octahedral chain structure in preference to structures that are either 3D and corner-sharing (i.e., perovskite) or 1D and face-sharing. $(Gua)_2PbI_4$ exhibits 2D corner-sharing octahedral connectivity in agreement with previous work. Density functional theory calculations are used to gain insight into the relative stabilities of the three polymorphs of $GuaPbI_3$ and to assess how the connectivity and dimensionality of the octahedral framework influence the electronic structure of each of the hybrid perovskites studied. https://doi.org/10.1063/1.5046404

Organic-inorganic lead halide perovskite materials, $[Am]PbX_3$ with Am = organic amine and X = Cl, Br, or I, are currently of great interest in the photovoltaic community due to dramatic improvements in their solar to electrical conversion efficiencies, which now exceed 22%.[1] One of the advantages of organic-inorganic perovskites is their ability to offer tuneable optical properties in the visible to infrared regions.[2] The ABX_3 perovskite architecture, which is characterised by a 3D arrangement of corner-sharing BX_6 octahedra, allows for many potential atom substitutions and this enables the spectral absorption range and other physical properties of the material to be adjusted and tailored.[3,4] The scope of such substitutions has recently been assessed in an extension of Goldschmidt's classical Tolerance Factor (TF) concept to hybrid perovskites.[5,6] Despite the excellent potential of hybrid lead perovskites, their susceptibility to thermal degradation and moisture absorption limits their use in practical devices.[7] As a consequence, perovskite-like structures which have reduced octahedral connectivity have attracted increasing attention due to their improved chemical stability.[8,9]

Most current research focuses on hybrid lead iodide perovskites with 3D octahedral connectivity since they exhibit the highest conversion efficiencies in photovoltaics.[10] Considering the size of the A-site cavity in an $APbI_3$ crystal, medium-sized organic cations, such as methylammonium (CNH_6, denoted MA) and formamidinium (CN_2H_5, denoted FA), crystallize in 3D perovskite forms. Smaller and larger cations, such as ammonium (NH_4) and ethylammonium (C_2NH_7, denoted EA), result in TFs less than 0.8 or greater than 1.0, respectively, and lead to the formation of lower dimensional architectures.[11,12] Interestingly, some of the amines that have TFs close to the 0.8 and 1.0 boundaries can crystallize in more than one polymorph.[13] For example, formamidinium lead iodide forms both a black 3D perovskite and a yellow trigonal perovskite-like structure with a 1D

[a]Authors to whom correspondence should be addressed: pdb1000@cam.ac.uk; akc30@cam.ac.uk; and shijings@mit.edu

octahedral arrangement that is face-sharing.[14] Similarly, $CsPbI_3$ undergoes a reconstructive phase transition from a 1D PbI_6 edge-sharing structure to a 3D corner-sharing perovskite between 560 and 600 K.[15,16] The study of polymorphisms is further motivated by the resulting changes in optical and electronic properties, although a few reports reveal the role of the organic cations in the formation of the resultant polymorphs.[17]

As an alternative to polar organic cations such as methylammonium, non-polar guanidinium (CN_3H_6, denoted Gua) forms an interesting range of halides. For instance, Stoumpos *et al.* determined the structures of $GuaGeI_3$ and $GuaSnI_3$ and found them to be hexagonal with 1D octahedral connectivity that is either face-sharing or a combination of face-sharing and corner-sharing.[17,18] Two compositions have been reported for guanidinium lead iodide, $GuaPbI_3$ and $(Gua)_2PbI_4$.[19–21] The triiodide has 1D octahedral connectivity, whereas for the tetraiodide it is 2D. The observed low dimensionality of these iodides is consistent with the TF of the 3D perovskite form of $GuaPbI_3$, which is 1.03.[5] Computationally, only the hypothetical 3D structure has been studied.[22] As a way of enhancing carrier mobility and chemical stability further, mixed cation perovskites involving guanidinium ions have also been synthesised.[23,24] For example, although devices employing pure $GuaPbI_3$ and $(Gua)_2PbI_4$ have yielded efficiencies of only 0.45%,[25] Soe *et al.* recently presented a series of low dimensional perovskites $(C(NH_2)_3)(CH_3NH_3)_nPb_nI_{3n+1}$ (n = 1, 2, and 3) using guanidinium and formamidinium as interspacers and achieved an efficiency of 7.26%.[26] With growing interest in adding guanidinium cations to lead iodide systems so as to modify their optical properties and film stability,[27] a thorough study of the structural characteristics and phase stability of Gua-based iodoplumbates is needed to guide the rational design of hybrid perovskite solar cell materials.

In the present work, we describe the synthesis, crystal structures, and a theoretical analysis of three Gua-based iodoplumbates. Our experimental results for $GuaPbI_3$ and $(Gua)_2PbI_4$ confirm the previous studies. In particular, $GuaPbI_3$ adopts the 1D NH_4CdCl_3-type connectivity at room temperature with edge-sharing octahedra and is labeled $GuaPbI_3$-e and $GuaPbI_3$-e_{RT} in Fig. 1. However, as discussed below, it undergoes a displacive phase transition upon cooling [labeled $GuaPbI_3$-e_{LT} in Fig. 1(b)] as a result of the reduced disorder of the guanidinium cations. $(Gua)_2PbI_4$ has 2D corner-sharing octahedral connectivity as previously reported,[20] but we have also synthesized a new composition, $(Gua)_3PbI_5$, which has 1D chains of corner-sharing octahedra (CCDC 1861695). To better understand the observations, we have performed a number of density functional theory (DFT)

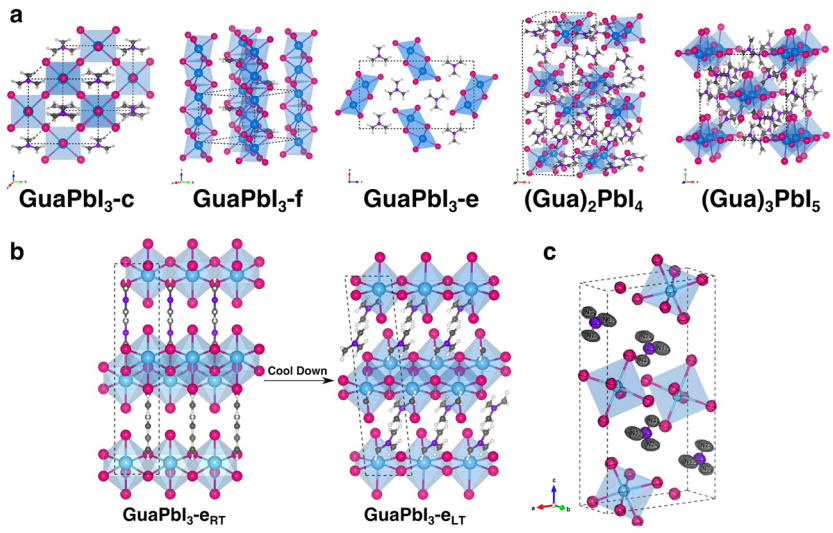

FIG. 1. (a) Two hypothetical polymorphs of $GuaPbI_3$ ($GuaPbI_3$-c and $GuaPbI_3$-f) and the observed structures of $GuaPbI_3$ ($GuaPbI_3$-e), $(Gua)_2PbI_4$, and $(Gua)_3PbI_5$ ("c," "f," and "e" denote corner-sharing, face-sharing, and edge-sharing inorganic octahedra, respectively). (b) Phase transition of $GuaPbI_3$-e on cooling from room temperature (RT) to 120 K (LT). (c) $GuaPbI_3$-e_{LT} showing the observed thermal ellipsoids of guanidinium and the tilting of the inorganic octahedra found from the DFT calculations. Atom colours: Pb: blue, I: pink, N: purple, C: gray, and H: silver.

calculations. In particular, we have compared the formation enthalpy of $GuaPbI_3$-e with two other hypothetical polymorphs, $GuaPbI_3$-c and $GuaPbI_3$-f, which exhibit corner-sharing and face-sharing octahedral connectivities, respectively [see Fig. 1(a)]. The structural properties of all three observed iodoplumbates are calculated and the band structures of $(Gua)_2PbI_4$ and $(Gua)_3PbI_5$ are compared to reveal the effects of octahedral connectivity and dimensionality on the electronic characteristics of this family of hybrid perovskites.

Single crystals of Gua-based iodoplumbates, $(Gua)_xPbI_{x+2}$ (x = 1, 2, and 3), were examined by single-crystal X-ray diffraction (SCXRD). The crystals were grown under the same experimental conditions as reported previously[27] for FA- and MA-based perovskites, and the different stoichiometries were obtained by tuning the ratio of Gua^+ and Pb^{2+} ions in the starting materials. For $GuaPbI_3$ and $(Gua)_2PbI_4$, pure phase crystals were readily obtained. For $(Gua)_3PbI_5$, mixed phase samples containing $(Gua)_3PbI_5$, $(Gua)_2PbI_4$, and $GuaPbI_3$ were harvested. Single crystals of $(Gua)_3PbI_5$ were collected from the mixture for structural characterization. The crystal structures were solved using SCXRD, primarily at room temperature. $GuaPbI_3$, which is yellow in colour and needle-like at room temperature, crystallizes in the orthorhombic space group, *Pnma*, with lattice parameters $a = 11.9987(8)$ Å, $b = 4.4693(4)$ Å, and $c = 20.874(2)$ Å, which is consistent with a recent powder X-ray diffraction (PXRD) study by Jodlowski *et al.*[21] The crystal adopts a 1D double chain structure, within which each Pb^{2+} ion is coordinated by six I-ions in a distorted octahedral environment. The PbI_6 octahedra are connected by common edges and arranged into double chains along the *b*-axis and the guanidinium ions fit in the spaces between the double chains, as shown in Fig. 1 ($GuaPbI_3$-e) and Fig. S2. There are three different kinds of Pb—I bonds with Pb—I distances ranging from 3.07 Å to 3.25 Å (terminal Pb—I_3 = 3.074 Å, two bridging bonds of Pb—I_2 = 3.207 Å, and three bridging bonds of Pb—I_1 = 3.246 Å and Pb—$I_1{}^1$ = 3.435 Å). The chain-like structure of $GuaPbI_3$ is of the type found in NH_4CdCl_3 and is isostructural with NH_4PbI_3[11] and the room temperature δ phase of $CsPbI_3$ and $RbPbI_3$[15] grown by the Bridgman technique.[28] Although the PbI_6 octahedra are observed to be distorted, there is no obvious stereo-chemical effect due to Pb lone pairs. The *cis* I—Pb—I angles vary between 87.0° and 93.6°, and the *trans* I_2—Pb—I_3 angles are 172.9°. $GuaPbI_3$-e was found to crystallize out quickly from the mother liquor and remain stable in air (HI aqueous solution) between 4 °C and 90 °C with tuned solution concentrations of the reactants. The SCXRD data collected for $GuaPbI_3$-e at 120 K show that a phase transition takes place on cooling and the resultant unit cell exhibits monoclinic symmetry with lattice parameters $a = 4.5737(4)$ Å, $b = 11.7901(9)$ Å, $c = 19.558(2)$ Å, and $\beta = 94.2°$. The inorganic framework retains the same double edge-sharing connectivity; however, heavy twinning upon cooling inhibited the accurate determination of the atomic positions of the light elements in the guanidinium ions (see Table SIII).

Crystals of $(Gua)_2PbI_4$ are orange and rectangular-shaped at room temperature and crystallize in space group $P2_1/n$ with lattice parameters $a = 9.2440(3)$ Å, $b = 26.9511(11)$ Å, $c = 12.7155(3)$ Å, and $\beta = 91.482(2)°$, which is consistent with previous work.[19] As shown in Figs. 1(a) and S3, the structure consists of double layers of corner-sharing octahedra with 2D connectivity. Gua cations fill the cavities between two polyhedra within a layer and between layers. The two adjacent polyhedra in the same layer along the *a*-axis are heavily tilted in order to accommodate a guanidinium cation, with the most distorted Pb—I—Pb angle being as low as 154.405(19)°. This indicates that the Gua cation is too large to fit in the perovskite cage and is consistent with the theoretical prediction using our tolerance factor approach. The concept of extending the Goldschmidt tolerance factor to hybrid perovskites and the method used to estimate the size of the organic cations are reliable and thus indicate that lone pair effects, which can produce a distorted 3D perovskite, are not as dominant as the size factor in this case, unlike in the Sn and Ge-based guanidinium perovskites mentioned previously.

$(Gua)_3PbI_5$ is yellow at room temperature and crystallizes in the monoclinic space group $C2/c$ with lattice parameters $a = 13.0694(5)$ Å, $b = 13.1946(5)$ Å, $c = 12.7212(5)$ Å, and $\beta = 91.276(4)°$. This composition has not been reported previously, and the structure is characterised by a PbI_6 network of corner-sharing octahedra forming 1D chains extending along the *c*-axis, as shown in Figs. 1(a) and S4. The octahedra are less distorted than in $GuaPbI_3$-e with Pb—I bond lengths ranging from 3.2123(6) to 3.2505(2) Å and a bridging Pb—I—Pb angle between two adjacent octahedra of 156.13(3)°. The $(Gua)_3PbI_5$ structure has the same inorganic connectivity as that reported for $(FA)_3PbI_5$ with space

TABLE I. DFT calculated structural properties of $(Gua)_xPbI_{x+2}$ (x = 1, 2, 3) compared with experimental measurements and a previous computational study.[22]

Structural properties	$GuaPbI_3$-c		$GuaPbI_3$-f	$GuaPbI_3$-e		$(Gua)_2PbI_4$		$(Gua)_3PbI_5$	
	3D corner-sharing		1D face-sharing	1D edge-sharing		2D corner-sharing		1D corner-sharing	
	DFT	DFT Giorgi *et al.*[22]	DFT	DFT	Expt.	DFT	Expt.	DFT	Expt.
a (Å)	9.37	9.34	9.44	12.16	11.99	9.23	9.24	13.32	13.07
b (Å)	9.37	9.34	9.44	4.37	4.47	27.05	26.95	12.92	13.19
c (Å)	10.35	10.33	7.81	20.63	20.87	12.65	12.72	12.44	12.72
α (deg)	90.00	89.60	90.00	90.00	90.00	90.00	90.00	90.00	90.00
β (deg)	90.00	90.40	90.00	90.00	90.00	91.18	91.48	90.00	91.28
γ (deg)	120.00	119.40	120.00	90.00	90.00	90.00	90.00	90.00	90.00
V per f.u. ($Å^3$)	261.97	262.03	300.18	274.22	279.81	394.45	395.85	535.22	548.29
ρ (g/cm^3)	4.20	4.11	3.58	3.92	3.85	3.52	3.50	3.17	3.50

group $P2_1/c$.[29,30] In addition, similar corner-sharing chains were observed in $[NH_2C(I)=NH_2]_3PbI_5$ by Wang and co-workers in the 1990s.[31]

The effective radius of Gua^+ (278 pm) is larger than that of either MA^+ (217 pm) or FA^+ (253 pm), which are the only two organic cations which form hybrid $[Am]PbI_3$ phases that adopt the 3D perovskite structure. As noted above, the TF of $GuaPbI_3$ in a 3D perovskite architecture is 1.03(9),[5] which is slightly above the limit for stability.[32] The effective radius of Gua^+ is comparable to that of EA^+ (274 pm), which forms the $EAPbI_3$ structure containing infinite chains of face-sharing PbI_6 polyhedra.[33] It is therefore interesting that $GuaPbI_3$ adopts an edge-sharing double chain structure instead of forming a face-sharing hexagonal structure like $EAPbI_3$.

The DFT-calculated structural properties of edge-sharing $GuaPbI_3$-e, two hypothetical corner-sharing and face-sharing structures $GuaPbI_3$-c and $GuaPbI_3$-f, as well as Gua_2PbI_4 and Gua_3PbI_5, are shown in Table I. The relaxed lattice parameters of $GuaPbI_3$-e, $(Gua)_2PbI_4$, and $(Gua)_3PbI_5$ agree well with our experimental measurements.

To understand better the structural stability of $GuaPbI_3$, we constructed two hypothetical polymorphs [Fig. 1(a)]: (i) a 3D corner-sharing perovskite structure $GuaPbI_3$-c and (ii) a 1D face-sharing structure, $GuaPbI_3$-f, isostructural with the two polymorphs of $FAPbI_3$ having space groups $P3m1$ and $P6_3mc$, respectively. The numbers of formula units per conventional unit cell of $GuaPbI_3$-c, $GuaPbI_3$-f, and $GuaPbI_3$-e are 3, 2, and 4, respectively. Our results for $GuaPbI_3$-c are in good agreement with a previous computational study[22] and those for $GuaPbI_3$-e are consistent with our experimental data (Table I). The three $GuaPbI_3$ polymorphs have similar stabilities in terms of enthalpy, as seen from Table II. The difference in formation enthalpy between $GuaPbI_3$-e and $GuaPbI_3$-c shows that $GuaPbI_3$-e is slightly more stable, with a difference of 6.41 kJ/mol per formula unit (f.u.). This value is 2 times larger than thermal energy at 298 K (2.48 kJ/mol per f.u.), which suggests that thermodynamically there is only a small difference between the enthalpies of the two structures. The formation enthalpy of $GuaPbI_3$-f is 11.32 kJ/mol per f.u. lower than that of the experimental structure, $GuaPbI_3$-e. It is therefore surprising that, although $GuaPbI_3$-f is predicted to be the most stable polymorph using DFT, experimentally $GuaPbI_3$-e is found at room temperature. However, by performing DFT relaxation on $GuaPbI_3$-e without applying any symmetry constraints, we

TABLE II. DFT-calculated relative formation enthalpies (ΔH_f) of $GuaPbI_3$.

Polymorph	ΔH_f (kJ/mol per f.u.)
$GuaPbI_3$-e ($GuaPbI\text{-}e_{RT}$)	11.41
$GuaPbI_3$-f	0.09
$GuaPbI_3$-c	17.82
$GuaPbI_3\text{-}e_{LT}$	0.00

obtained a lower symmetry structure ($GuaPbI_3$-e_{LT}) with space group $P2_1/c$. The guanidinium cations in $GuaPbI_3$-e are aligned perpendicular to the chain direction (b-axis), whereas in $GuaPbI_3$-e_{LT} they are tilted [Fig. 1(b)]. Importantly, we confirmed the experimental stability of this structure using low temperature (120 K) SCXRD, i.e., a transformation into the $P2_1/c$ structure was observed on cooling. As indicated by the thermal ellipsoids derived from the SCXRD [Fig. 1(c)], the guanidinium cations are clearly tilted, in agreement with our DFT results. The DFT-calculated formation enthalpy of $GuaPbI_3$-e_{LT} is slightly lower than that of $GuaPbI_3$-f (0.09 kJ/mol per f.u.). However, this enthalpy difference is still much smaller than kT at room temperature (2.48 kJ/mol per f.u.). Therefore, there must be other reasons for the relative stabilities of these structures, such as synthesis environment, entropy, and kinetics. On cooling to 120 K, $GuaPbI_3$-e_{LT} forms a greater number of hydrogen bonds to stabilize the structure (see Fig. S5) and this lowers both its symmetry and enthalpy. As a consequence, entropy must play a role in stabilizing $GuaPbI_3$-e at room temperature. A previous study on the phase behavior of metal organic frameworks has attributed the observed polymorphs to entropic differences caused by hydrogen bonding and density.[34] Comparing the calculated densities of the three $GuaPbI_3$ polymorphs (Table I), the following trend is observed: $GuaPbI_3$-f < $GuaPbI_3$-e < $GuaPbI_3$-c. This would suggest the possibility that the lowest density/highest entropy $GuaPbI_3$-f phase might form at higher temperatures.

It is well known that hydrogen bonding, in particular, H···I bonding, plays an important role in determining the structure and stability of hybrid halide perovskites, where it can affect, for example, the degree of octahedral tilting.[35] Experimentally, the positions of the hydrogen atoms are difficult to determine using XRD with a material containing heavy elements such as Pb and I. However, DFT can be employed to calculate these positions together with various interatomic distances and bond angles, which can be used as indicators of bond strengths. In this work, we use the calculated I···N interatomic distances and N—H···I bond angles for this purpose. As shown in Fig. S5, $d_{I\cdots N}$ and ∠N—H···I distances and angles for every system studied in the present work vary between 3.6-4.0 Å and 100°-170°, respectively. This indicates an intermediate level of hydrogen bonding strength (compared, for example, with $MAPbI_3$, where the distances are ∼3.5-3.6 Å[35]). Interactions in the lower dimensional structures like $(Gua)_2PbI_4$ and $(Gua)_3PbI_5$ which contain a multiple number of Gua cations are complex, as shown from the $d_{I\cdots N}$ and ∠N—H···I distributions. For each guanidinium cation, there are 6, 12, 6, 10.5, and 9.3 hydrogen bonds associated with the $GuaPbI_3$-e, $GuaPbI_3$-c, $GuaPbI_3$-f, $(Gua)_2PbI_4$, and $(Gua)_3PbI_5$ structures, respectively. Comparing the bond lengths and bond angles of the three polymorphs of $GuaPbI_3$ in Fig. S5, we see that most of the H bonds in $GuaPbI_3$-e are weaker than in $GuaPbI_3$-c and $GuaPbI_3$-f.

DFT-calculated electronic band structures, along with their projected densities of states (PDOS), are shown in Fig. 2 and include spin-orbit coupling (SOC). The calculated bandgaps, with and without SOC, are compared with the measured values in Table SII. For the $GuaPbI_3$ series, $GuaPbI_3$-c, $GuaPbI_3$-e, and $GuaPbI_3$-f have calculated SOC bandgaps of 0.36 eV, 2.27 eV, and 2.50 eV, respectively, which compare with a measured value of 2.57 eV for $GuaPbI_3$-e. For $(Gua)_2PbI_4$ and $(Gua)_3PbI_5$, the SOC bandgaps are 1.52 eV and 1.94 eV, respectively, while the measured value for $(Gua)_2PbI_4$ is 2.47 eV. In general, the calculated values are smaller than the measured ones, as expected for DFT + SOC. The PDOS indicates that the band edges are dominated by Pb-6s, 6p, and I-5p states that originate from the Pb—I inorganic framework. The inorganic and organic (Gua) states are well decoupled at the band edges. There are two factors in the present study that can influence the electronic properties significantly: (i) the connectivity and (ii) the dimensionality of the inorganic Pb—I framework. Pb—I connectivity will change the orbital overlaps and hence the average Pb—I—Pb bond angles, as shown in Fig. 3. For the three polymorphs of $GuaPbI_3$, it is seen that the bandgaps decrease as the connectivity changes from face-sharing to edge-sharing to corner-sharing, while at the same time the bond angles increase. Dimensionality affects electronic properties by the confinement of forming Pb—I chains or planes, which usually increases the bandgap as the dimensionality decreases. Therefore, we expect the bandgap to follow the following trend: face-sharing > edge-sharing > corner-sharing and 1D > 2D > 3D, which is clearly seen in Fig. 3. From the band structures shown in Fig. 2, directions that are quantum confined (e.g., the direction perpendicular to the $[PbI_3]^-$ chains in $GuaPbI_3$-e) show more flat band dispersion (e.g., from Γ-Y-A-B in $GuaPbI_3$-e). A similar trend has also been reported recently in Sn-based low-dimensional

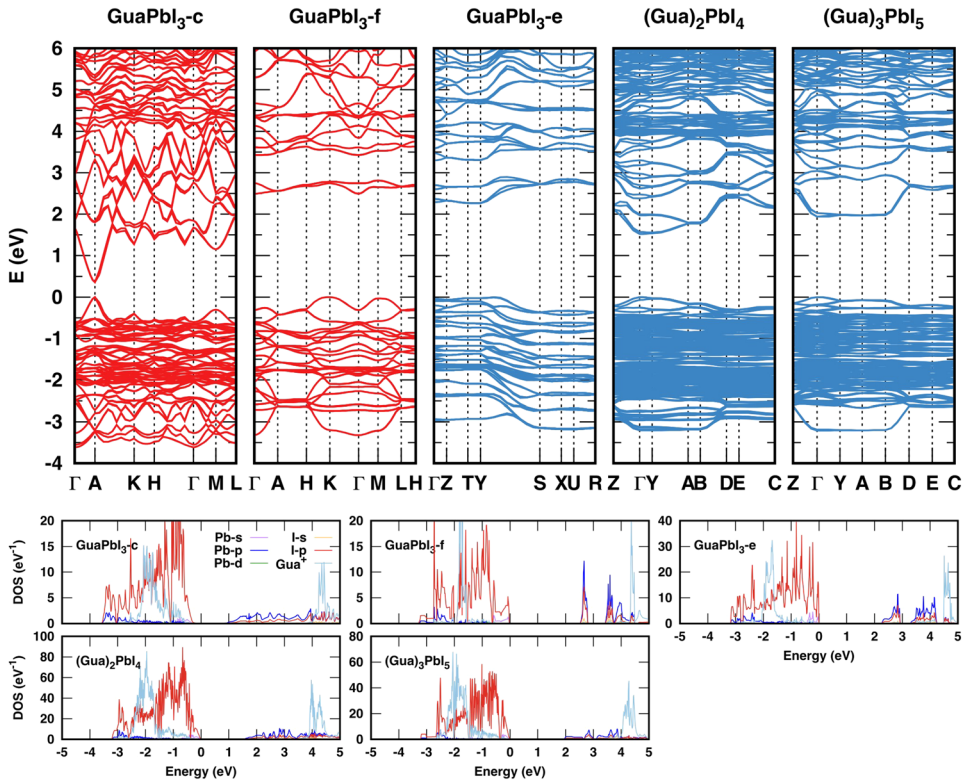

FIG. 2. DFT-calculated electronic band structures (red plots are hypothetical structures and blue plots are for those experimentally observed) and their projected densities of states (PDOS) considering spin-orbit coupling (SOC). Following high symmetric paths are used: $GuaPbI_3$-c: Γ(0,0,0)-A(0,0,0.5)-H(−0.3333,0.6667,0.5)-K(−0.3333,0.6667,0)-Γ(0,0,0)-M(0,0.5,0)-L(0,0.5,0.5)-H(−0.3333,0.6667,0.5); $GuaPbI_3$-f: Γ(0,0,0)-A(0,0,0.5)-H(−0.3333,0.6667,0.5)-K(−0.3333,0.6667,0)-Γ(0,0,0)-M(0,0.5,0)-L(0,0.5,0.5)-H(−0.3333,0.6667,0.5); $GuaPbI_3$-e: Γ(0,0,0)-Z(0,0,0.5)-T(−0.5,0,0.5)-Y(−0.5,0,0)-S(−0.5,0.5,0)-X(0,0.5,0)-U(0,0.5,0.5)-R(−0.5,0.5,0.5); Gua_2PbI_4 and Gua_3PbI_5: Z(0,0,0.5)-Γ(0,0,0)-Y(0,0.5,0)-A(−0.5,0.5,0)-B(−0.5,0,0)-D(−0.5,0,0.5)-E(−0.5,0.5,0.5)-C(0,0.5,0.5).

perovskites.[17] Connectivity and dimensionality also affect relativistic interactions. Table SII shows that the computed differences in the bandgap (ΔE_g) for each structure with and without SOC increase as the bandgap decreases. However, ΔE_g for $(Gua)_3PbI_5$ is smaller than that for $GuaPbI_3$-e. This

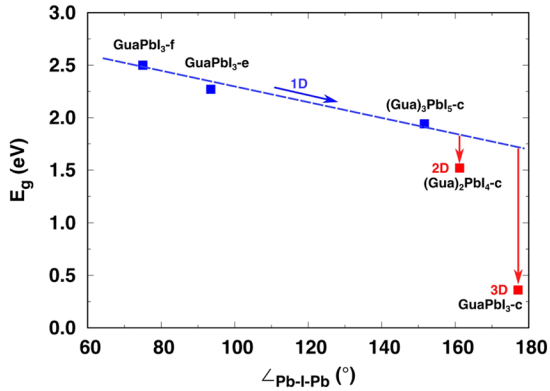

FIG. 3. DFT-calculated bandgaps (E_g including SOC) as a function of the averaged Pb–I–Pb bond angles in $(Gua)_xPbI_{x+2}$ (x = 1, 2, and 3) using the data in Table SI. "c," "f," and "e" denote $GuaPbI_3$ structures with corner-sharing, face-sharing, and edge-sharing octahedral, respectively. $GuaPbI_3$-f and $GuaPbI_3$-c are hypothetical structures. Structures with 1D octahedral connectivity are shown with blue symbols whereas those with 2D connectivity ($(Gua)_2PbI_4$) and 3D connectivity ($GuaPbI_3$-c) are shown with red symbols. The red arrows show the effect of quantum confinement in 2D (~0.25 eV) and 3D (~1.25 eV) compared to 1D structures.

is because $GuaPbI_3$-e has a double-chain instead of a single-chain structure so that the relativistic effect is larger in $GuaPbI_3$-e. This is an excellent illustration of how to tune the bandgap of a hybrid perovskite by controlling the connectivity and dimensionality of the inorganic framework.

This study has presented a combined experimental and computational analysis of the effects of octahedral connectivity and dimensionality on the stabilities of three guanidinium-based iodoplumbates. The SCXRD experiments show that $GuaPbI_3$ has 1D edge-sharing octahedral connectivity, $(Gua)_2PbI_4$ has 2D corner-sharing octahedral connectivity, and $(Gua)_3PbI_5$ has 1D corner-sharing octahedral connectivity. $(Gua)_3PbI_5$ is a new composition whereas $GuaPbI_3$ and $(Gua)_2PbI_4$ have been synthesised previously. The measured bandgap of $(Gua)_2PbI_4$ is smaller than that of $GuaPbI_3$. DFT calculations of the structure of the three iodoplumbates are consistent with the measurements and, in particular, confirm the stability of the low temperature form of $GuaPbI_3$ with $P2_1/c$ symmetry. Calculations of the formation enthalpies of two other hypothetical polymorphs of $GuaPbI_3$, one with 1D face-sharing connectivity and the other with 3D corner-sharing connectivity, suggest that entropy must play a role in stabilising the observed form of $GuaPbI_3$ with *Pnma* symmetry at room temperature. The calculated band structures of the iodoplumbates confirm that their bandgaps increase with reducing dimensionality due to quantum confinement effects. Octahedral connectivity is also shown to affect the bandgap, with face-sharing octahedra resulting in the largest bandgap. Overall, the results add to our knowledge of the effects of connectivity and dimensionality on the stabilities and electronic properties of hybrid perovskites, particularly those that are guanidinium based, and may motivate further studies on mixed cation perovskites in the rational design of materials for photovoltaic devices.

One of the precursors, guanidinium iodide ($C(NH_2)_3I$), was first prepared by adding guanidinium carbonate (8.03 g) to hydriodic acid (HI) (20 g, aqueous solution, 57 wt. %) in equal molar amounts. A white solid was obtained after removing water at 50 °C using a rotational evaporator. The product was stored in an argon glove box. Single crystals of $GuaPbI_3$ and $(Gua)_2PbI_4$ suitable for single-crystal X-ray diffraction were prepared using an adaptation of the Poglitsch and Weber method[36] in which lead iodide (Sigma-Aldrich) is reacted with stoichiometric solid guanidinium iodide in aqueous (57%) HI solution. The crystals could also be produced using lead acetate trihydrate instead of lead iodide. Lead acetate trihydrate (379 mg, 1 mmol) was added to the flask and dissolved in 1 ml HI solution upon heating to 120 °C and 1 mmol of solid $C(NH_2)_3I$ was added. The solution was then left to cool to 25 °C and transferred onto a crystallization dish. Yellow precipitates were collected upon evaporation of the solvent. The precipitates were found to contain a mixture of $GuaPbI_3$, $(Gua)_2PbI_4$, and $(Gua)_3PbI_5$ single crystals.

The resulting yellow needle-like, rectangular-shaped and prism-shaped crystals (see Fig. S1) were characterised by single crystal diffractometry using an Oxford Diffraction Gemini A Ultra X-ray diffractometer with Mo Kα radiation (λ = 0.7093 Å). CrysAlisPro software (Agilent Technologies) was used for data collection and reduction, unit cell determination and refinement, and applying the face-based analytical absorption correction. The structure of $GuaPbI_3$ was solved by direct methods with SHELX in the Olex2 platform. All non-hydrogen atoms were refined anisotropically and hydrogen atoms were then added at the calculated positions. The crystal data are summarized in Table III (cif files are attached in the ESI).

Optical bandgap measurements were performed on a PerkinElmer Lambda 750 UV-Visible spectrometer in reflectance mode with a 2 nm slit width, a 1 nm interval, and a wavelength range between 300 and 1200 nm. Bulk samples for UV-Vis measurement were prepared by grinding the $GuaPbI_3$ and $(Gua)_2PbI_4$ single crystals into fine powders. Measurements on $(Gua)_3PbI_5$ were not made because it was phase impure. The bandgap was estimated using the Tauc method by converting the reflectance into a Kubelka-Munk function and plotting it against photon energy, hν (Fig. S6).

The DFT calculations were performed using projector-augmented wave (PAW)[37,38] pseudopotentials with the valence electrons from Pb ($5d^{10}6s^26p^2$), I ($5s^25p^5$), C ($2s^22p^2$), N ($2s^22p^3$), and H ($1s^2$) treated explicitly. The PBEsol exchange-correlation functional was employed together with spin-orbit coupling (SOC). The complete methodology is implemented in the VASP code.[39,40] A 500 eV plane wave kinetic energy cutoff was used for all calculations and 3 × 9 × 2, 3 × 3 × 3, 3 × 3 × 3, 4 × 2 × 3, and 3 × 3 × 3 gamma centered k-point meshes were used for $GuaPbI_3$-e, $GuaPbI_3$-c, $GuaPbI_3$-f, $(Gua)_2PbI_4$, and $(Gua)_3PbI_5$ using the Monkhorst-Pack method. Formation

TABLE III. Crystallographic data and refinements of $(Gua)_3PbI_5$, $(Gua)_2PbI_4$, and $GuaPbI_3$ structures.

Empirical formula[a]	$C_3I_5N_9H_{18}Pb$	$C_2I_4N_6H_{12}Pb$	$CI_3N_3H_6Pb$
Formula weight	1021.95	834.97	641.93
Temperature (K)	297.5(5)	293(2)	299.7(6)
Crystal system	Monoclinic	Monoclinic	Orthorhombic
Space group	C2/c	$P2_1/n$	Pnma
a (Å)	13.0694(5)	9.2440(3)	11.9866(5)
b (Å)	13.1946(5)	26.9511(11)	4.4740(2)
c (Å)	12.7212(5)	12.7155(3)	20.8652(10)
α (deg)	90	90	90
β (deg)	91.276(4)	91.482(2)	90
γ (deg)	90	90	90
Volume ($Å^3$)	2193.18(15)	3166.82(17)	1118.96(9)
Z	4	8	4
ρ_{calc} (g/cm^3)	3.095	3.503	3.81
μ (mm^{-1})	14.732	18.433	23.293
F(000)	1784	2 880	1072
Crystal size (mm^3)	0.17 × 0.09 × 0.06	0.35 × 0.11 × 0.06	0.72 × 0.08 × 0.07
2Θ range (deg)	4.388–56.64	3.542–56.848	3.904–46.496
Index ranges	$-17 \le h \le 11$, $-11 \le k \le 17$, $-16 \le l \le 14$	$-9 \le h \le 12$, $-35 \le k \le 15$, $-17 \le l \le 13$	$-13 \le h \le 11$, $-4 \le k \le 4$, $-22 \le l \le 23$
Reflections collected	4425	12 954	5700
Independent reflections	2433 [R_{int} = 0.0284, R_{sigma} = 0.0413]	6 990 [R_{int} = 0.021 2, R_{sigma} = 0.034 2]	918 [R_{int} = 0.0403, R_{sigma} = 0.0256]
Data/restraints/parameters	2433/0/103	6990/1/235	918/0/40
Goodness-of-fit on F^2	1.056	1.186	1.018
Final R indexes [I >= 2σ (I)]	R_1 = 0.0367, wR_2 = 0.0784	R_1 = 0.030 1, wR_2 = 0.066 7	R_1 = 0.0216, wR_2 = 0.0482
Final R indexes (all data)	R_1 = 0.0547, wR_2 = 0.0868	R_1 = 0.036 5, wR_2 = 0.068 7	R_1 = 0.0258, wR_2 = 0.0500
Largest diff. peak/hole (e $Å^{-3}$)	1.16/−1.06	2.27/−1.88	0.80/−0.81

[a]H positions shown in the formula were not considered in the structural solution due to the difficulty of detecting light H in the presence of heavy Pb and I with X-ray diffraction.

enthalpies (H_f) of $GuaPbI_3$-e, $GuaPbI_3$-c, and $GuaPbI_3$-f were calculated using $H_f = E(GuaPbI_3)$-E(C)-3E(N)-6E(H)-E(Pb)-3E(I), where $E(GuaPbI_3)$ is the total energy per formula unit of $GuaPbI_3$ and E(C), E(N), E(H), E(Pb), and E(I) are the total energies per atom of the elements using standard state structures. Here we used graphite, nitrogen gas, hydrogen gas, fcc lead, and orthorhombic iodine and all the gas phases were optimized by placing a dimer in a 15 × 15 × 15 $Å^3$ box in a gamma k-point calculation. The relative formation enthalpy ΔH_f was determined by setting the lowest H_f to zero. The crystal structures were visualized using the VESTA code.[41]

See supplementary material for Figs. S1–S6, Tables SI, SII, and SIII, and crystal structures of $GuaPbI_3$-e, $GuaPbI_3$-eLT, Gua_2PbI_4, and Gua_3PbI_5.

S.S., G.K., and A.K.C. thank the Ras Al Khaimah Center for Advanced Materials for financial support. G.K. further acknowledges support from the DFG (No. KI1870). Z.D. is grateful to the Cambridge Overseas Trust and the China Scholarship Council for their support. The authors would like to thank Linjie Dai for help with the UV-vis measurements. The calculations were performed at the Cambridge HPCS and the UK National Supercomputing Service, ARCHER. Access to the latter was obtained via the UKCP consortium and funded by EPSRC under Grant No. EP/P022596/1.

The open access computational data are available at https://doi.org/10.17863/CAM.26381.

[1] National Renewable Energy Laboratory (NREL) Best Research-Cell Efficiencies, National Renewable Energy Laboratory, Best Research-Cell Efficiencies.
[2] A. Walsh, J. Phys. Chem. C **119**, 5755–5760 (2015).
[3] Q. Chen, N. De Marco, Y. Michael Yang, T.-B. Song, C.-C. Chen, H. Zhao, Z. Hong, H. Zhou, and Y. Yang, Nano Today **10**, 355 (2015).
[4] L. Dong, S. Sun, Z. Deng, W. Li, F. Wei, Y. Qi, Y. Li, X. Li, P. Lu, and U. Ramamurty, Comput. Mater. Sci. **141**, 49–58 (2018).

[5] G. Kieslich, S. Sun, and A. K. Cheetham, Chem. Sci. **5**, 4712–4715 (2014).
[6] G. Kieslich, S. Sun, and A. K. Cheetham, Chem. Sci. **6**, 3430–3433 (2015).
[7] G. Divitini, S. Cacovich, F. Matteocci, L. Cinà, A. Di Carlo, and C. Ducati, Nat. Energy **1**, 15012 (2016).
[8] Q. Jiang, D. Rebollar, J. Gong, E. L. Piacentino, C. Zheng, and T. Xu, Angew. Chem. **127**, 7727–7730 (2015).
[9] D. H. Cao, C. C. Stoumpos, O. K. Farha, J. T. Hupp, and M. G. Kanatzidis, J. Am. Chem. Soc. **137**, 7843–7850 (2015).
[10] M. A. Green and A. Ho-Baillie, ACS Energy Lett. **2**, 822–830 (2017).
[11] L.-Q. Fan and J.-H. Wu, Acta Crystallogr., Sect. E: Struct. Rep. Online **63**, i189 (2007).
[12] M. Safdari, A. Fischer, B. Xu, L. Kloo, and J. M. Gardner, J. Mater. Chem. A **3**, 9201–9207 (2015).
[13] N. J. Jeon, J. H. Noh, W. S. Yang, Y. C. Kim, S. Ryu, J. Seo, and S. Il Seok, Nature **517**, 476–480 (2015).
[14] C. C. Stoumpos, C. D. Malliakas, and M. G. Kanatzidis, Inorg. Chem. **52**, 9019–9038 (2013).
[15] D. M. Trots and S. V. Myagkota, J. Phys. Chem. Solids **69**, 2520–2526 (2008).
[16] J. Brgoch, A. J. Lehner, M. Chabinyc, and R. Seshadri, J. Phys. Chem. C **118**, 27721–27727 (2014).
[17] C. C. Stoumpos, L. Mao, C. D. Malliakas, and M. G. Kanatzidis, Inorg. Chem. **56**, 56–73 (2017).
[18] C. C. Stoumpos, L. Fraser, D. J. Clark, Y. S. Kim, S. H. Rhim, A. J. Freeman, J. B. Ketterson, J. I. Jang, and M. G. Kanatzidis, J. Am. Chem. Soc. **137**, 6804–6819 (2015).
[19] M. Szafrański, Thermochim. Acta **307**, 177–183 (1997).
[20] M. Szafrański and A. Katrusiak, Phys. Rev. B **61**, 1026 (2000).
[21] A. D. Jodlowski, A. Yepez, R. Luque, L. Camacho, and G. de Miguel, Angew. Chem., Int. Ed. **55**, 14972–14977 (2016).
[22] G. Giorgi, J. I. Fujisawa, H. Segawa, and K. Yamashita, J. Phys. Chem. C **119**, 4694–4701 (2015).
[23] L. Dimesso, A. Quintilla, Y.-M. Kim, U. Lemmer, and W. Jaegermann, Mater. Sci. Eng. B **204**, 27–33 (2016).
[24] N. De Marco, H. Zhou, Q. Chen, P. Sun, Z. Liu, L. Meng, E.-P. Yao, Y. Liu, A. Schiffer, and Y. Yang, Nano Lett. **16**, 1009–1016 (2016).
[25] S. A. Kulkarni, T. Baikie, S. Muduli, R. Potter, S. Chen, F. Yanan, P. Bishop, S. S. Lim, T. C. Sum, N. Mathews, and T. J. White, Jpn. J. Appl. Phys., Part 2 **56**, 08MC05 (2017).
[26] C. M. M. Soe, C. C. Stoumpos, M. Kepenekian, B. Traoré, H. Tsai, W. Nie, B. Wang, C. Katan, R. Seshadri, A. D. Mohite, J. Even, T. J. Marks, and M. G. Kanatzidis, J. Am. Chem. Soc. **139**, 16297–16309 (2017).
[27] O. Nazarenko, M. R. Kotyrba, S. Yakunin, M. Aebli, G. Rainò, B. M. Benin, M. Wörle, and M. V. Kovalenko, J. Am. Chem. Soc. **140**, 3850–3853 (2018).
[28] I. N. Flerov, M. V. Gorev, K. S. Aleksandrov, A. Tressaud, J. Grannec, and M. Couzi, Mater. Sci. Eng.: R: Rep. **24**, 81–151 (1998).
[29] K. Tanaka, R. Ozawa, T. Umebayashi, K. Asai, K. Ema, and T. Kondo, Phys. E **25**, 378–383 (2005).
[30] K. D. Karlin, *Progress in Inorganic Chemistry* (John Wiley & Sons, Inc., Hoboken, NJ, USA, 1996), Vol. 48.
[31] S. Wang, D. B. Mitzi, C. A. Feild, and A. Guloy, J. Am. Chem. Soc. **117**, 5297–5302 (1995).
[32] A. M. Glazer, Acta Crystallogr., Sect. B: Struct. Crystallogr. Cryst. Chem. **28**, 3384–3392 (1972).
[33] J.-H. Im, J. Chung, S.-J. Kim, and N.-G. Park, Nanoscale Res. Lett. **7**, 353 (2012).
[34] A. K. Cheetham, G. Kieslich, and H. H.-M. Yeung, Acc. Chem. Res. **51**, 659–667 (2018).
[35] J.-H. Lee, N. C. Bristowe, P. D. Bristowe, and A. K. Cheetham, Chem. Commun. **51**, 6434–6437 (2015).
[36] A. Poglitsch and D. Weber, J. Chem. Phys. **87**, 6373 (1987).
[37] P. E. Blöchl, Phys. Rev. B **50**, 17953–17979 (1994).
[38] G. Kresse and D. Joubert, Phys. Rev. B **59**, 1758–1775 (1999).
[39] G. Kresse and J. Furthmüller, Phys. Rev. B **54**, 11169–11186 (1996).
[40] J. P. Perdew, A. Ruzsinszky, G. I. Csonka, O. A. Vydrov, G. E. Scuseria, L. A. Constantin, X. Zhou, and K. Burke, Phys. Rev. Lett. **100**, 136406 (2008).
[41] K. Momma and F. Izumi, J. Appl. Crystallogr. **44**, 1272–1276 (2011).